Computers and Geotechnics 140 (2021) 104447

Contents lists available at ScienceDirect

Computers and Geotechnics

journal homepage: www.elsevier.com/locate/compgeo

Coupled hydro-mechanical analysis of compacted bentonite behaviour during hydration

Jose A. Bosch [a], Alessio Ferrari [a,b], Lyesse Laloui [a]

[a] Swiss Federal Institute of Technology in Lausanne. EPFL ENAC IIC LMS, Station 18, 1015 Lausanne, Switzerland
[b] Università degli Studi di Palermo. Palermo, Italy

ARTICLE INFO

Keywords:
Bentonite
Hydro-mechanical couplings
Elasto-plasticity
Water retention
Unsaturated soils

ABSTRACT

This study analyses the response of compacted bentonites upon hydration based on a coupled hydro-mechanical elasto-plastic framework. As an alternative to multi-porosity interpretation, the framework was selected based on the experimental evidence of adsorbed water behaviour in bentonites and the volumetric response at saturated states, apparently independent of its initial state. Based on these premises, a water retention model was formulated using an explicit distinction between adsorbed water and free water, enabling the postulation of the water properties and behaviour depending on its state. In order to effectively account for the transition between unsaturated to saturated state, that can occur in a wide range of suctions, the stress–strain constitutive equations are written in terms of an effective stress and degree of saturation framework. The mathematical formulation was implemented in a finite element code and used to simulate and interpret the behaviour of MX-80 bentonite compacted in different forms during hydration for several stress paths, including loading and unloading cycles after saturation. A good agreement of the model with experimental results was obtained using a consistent set of parameters describing the saturated state behaviour. The typical non-linear swelling pressure development was interpreted through the two-way coupling between the water retention behaviour and elasto-plastic compressibility. The possible high suctions at saturated states explain the swelling potential after full hydration. Overall, this study offers new perspectives on the role of hydro-mechanical interactions in bentonite behaviour upon hydration.

1. Introduction

Bentonites are clays that contain a significant proportion of smectite minerals. Because of their solute retention capacity, low hydraulic conductivity, and self-healing capacity provided by their swelling potential, bentonites are typically used as buffer and sealing materials in deep geological repositories for nuclear waste (Sellin and Leupin, 2013). The swelling potential and hydraulic conductivity of bentonites are strongly related to their dry density. Thus, mathematical formulations for predicting the performance of geological repositories need to reproduce the mechanical behaviour of compacted bentonite upon hydration accurately.

It is widely accepted that two constitutive stress variables are required to model unsaturated soil behaviour (Houlsby, 1997; Jommi, 2000; Gens, 2010). Recent models for variably saturated and low-activity clays tend to use a first stress variable that depends on the water retention (WR) curve, the most common being the so called 'average skeleton stress' (Jommi, 2000) or 'generalised effective stress' (Nuth and Laloui, 2008). Because this variable controls the rate of elastic strains development, a direct relationship between WR and mechanical behaviour has been established, which is supported in several experimental studies (Gallipoli et al., 2003a; Wheeler et al., 2003; François and Laloui, 2008; Romero and Jommi, 2008), achieving a consistent hydro-mechanical interpretation with a reduced number of material parameters. The second stress variable is incorporated to express the soil compressibility dependency and yield stress on the current suction or saturation state (Alonso et al., 1990). Zhou et al. (2012a) presented a series of arguments supporting the application of the degree of saturation instead of suction, such as a natural decrease in the wetting-collapse potential at high stress and the natural transition from unsaturated to saturated states in compression paths.

Although it is expected that the same hydro-mechanical interactions apply to bentonite behaviour, most studies on bentonite ignored the coupling between WR and mechanical behaviour (Gens and Alonso, 1992; Alonso et al., 1999; Sánchez et al., 2005; Gens et al., 2011; Mokni et al., 2020; Navarro et al., 2020). Instead, constitutive models for

E-mail addresses: jose.boschllufriu@epfl.ch (J.A. Bosch), alessio.ferrari@epfl.ch (A. Ferrari), lyesse.laloui@epfl.ch (L. Laloui).

https://doi.org/10.1016/j.compgeo.2021.104447
Received 17 March 2021; Received in revised form 11 August 2021; Accepted 4 September 2021
Available online 15 September 2021

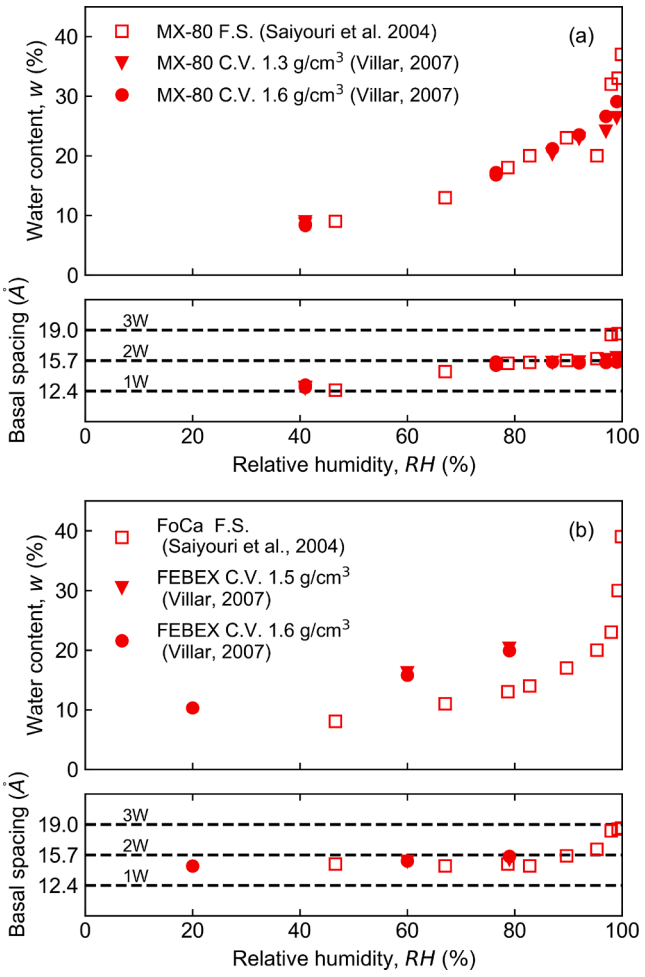

Fig. 1. Water content and average basal spacing obtained from interpretation of X-ray analysis as a function of *RH* on a) MX-80 bentonite (data from Saiyouri et al. (2004) and Villar (2007)), and b) FoCa clay (data from Saiyouri et al. (2004)) and Febex bentonite (data from Villar (2007)). F.S. denotes free swelling conditions, and C.V. denotes constant volume conditions. All tests involved an increase in RH from initial compacted conditions. Density values refer to the dry densities of the samples. Dashed lines refer to the theoretical spacing of 1, 2, and 3 water layer (W) hydration states.

analysing highly expansive soils are focused on incorporating the fabric observed in these materials (Lloret et al., 2003; Seiphoori et al., 2014; Ferrari et al., 2014) by dividing it into macro-porosity and micro-porosity. Hence, several features of expansive soil behaviour, particularly regarding the stress-path dependency, are interpreted on the basis of microstructure expansion and fabric rearrangement (Lloret et al., 2003; Sánchez et al., 2005; Gens et al., 2011). Although it is a convenient modelling framework, some aspects such as the state variables and parameters related to the microstructure and the interactions between structural levels require observations and measurements that may be difficult to obtain and validate.

Constitutive models for low and moderately expansive clays considering both hydro-mechanical and multiscale coupling have also been developed (Della Vecchia and Romero 2013, Mašín, 2013, Qiao et al., 2019). However, these models describe water retention behaviour as a function of the water stored in the microstructural voids, that is assumed not to be affected by volume changes. Because the micro-voids in bentonite can considerably expand on swelling, this hypothesis may lead to a significant discrepancy with the actual volume of adsorbed water, that does not exceed 3 or 4 molecular layers beyond the clay surface (Saiyouri et al., 2004).

This study addresses the interpretation and modelling of the hydro-mechanical behaviour of compacted bentonite-based materials by dividing the water ratio into adsorbed and free water using a single mechanical void ratio. The paper begins with a review of the experimental data that support two main arguments favouring this approach.

- The kinetics of interlayer adsorbed water can be modelled as a single function of relative humidity (*RH*) up to two layers of adsorbed water, supporting the separation of adsorbed water from free water, not only for the hydraulic problem (Revil and Lu, 2013), but also for the mechanical coupling.
- The volumetric behaviour in saturated states appears to be independent of the initial compacted state (e.g. compacted blocks, pellets, and powder), supporting the use of a single void ratio in the saturated state and the importance of a seamless transition between unsaturated and saturated states.

Some essential modifications of existing models were made to incorporate these observations. The water retention model developed by Revil and Lu (2013) was extended to include the mechanical coupling of free water behaviour. A generalised effective stress and the degree of saturation are used as constitutive stresses. Instead of the capillary degree of saturation (Zhou et al., 2018), the total degree of saturation was used as the Bishop parameter (Schrefler, 1984), resulting in natural incorporation of the swelling potential caused by the adsorbed water volume into the stress–strain equations. Because in highly compacted bentonites the transition between unsaturated and saturated states occurs at relatively high suction, and varies significantly with the void ratio, the degree of saturation is used as the variable that controls the yield surface in unsaturated states.

The formulation was implemented in the finite element code LAGAMINE (Charlier, 1987; Collin et al., 2002), and laboratory tests on Wyoming MX80 bentonite subjected to hydration in two different compaction states were simulated. A single set of material parameters for saturated states calibrated independently was used for both materials. The first analysis involved two swelling pressure tests on pellet/powder bentonite mixtures monitored extensively, including radial stress and *RH* at various distances from the wetting front (Bernachy-Barbe, 2021). The second analysis involved experimental tests for cycles of swelling pressure, unloading, and swelling related to the ability of saturated bentonite to seal technological gaps (Dueck et al., 2011).

2. Rheological evidence

2.1. Adsorbed water in bentonites

Because of its high content in smectite minerals compared to other clays, adsorbed water in bentonites is mainly stored through interlayer adsorption, which results from the combination of surface adsorption and cation hydration (Low, 1980; Yong, 1999). Up to three or four molecular layers of water can be adsorbed through this mechanism, which gradually increases with *RH* (Holmboe et al., 2012; Seiphoori et al., 2014). Water in the first two layers (the bi-hydrated state) shows a different structure and properties, such as density and viscosity, compared to bulk water (Sposito and Prost, 1982; Zhang and Lu, 2018). The interlayer adsorption process has been investigated through X-ray diffraction and neutron scattering under constant-volume hydration and unconstrained swelling conditions (Saiyouri et al., 2004; Devineau et al., 2006; Holmboe et al., 2012; Villar et al., 2012; Bestel, 2014).

Some cited interpretations of interlayer water during hydration are shown in Fig. 1. The data correspond to FoCa, FEBEX, and MX-80 bentonites, which either enabled free swelling (Saiyouri et al., 2004) or prevented volume change during hydration (Villar, 2007). For bentonites under free swelling conditions, the adsorption of the third layer of water occurs at *RH* close to 100%. However, there appears to be some uncertainty regarding the confinement conditions under which the third layer of adsorbed water develops. Contrary to the observations by

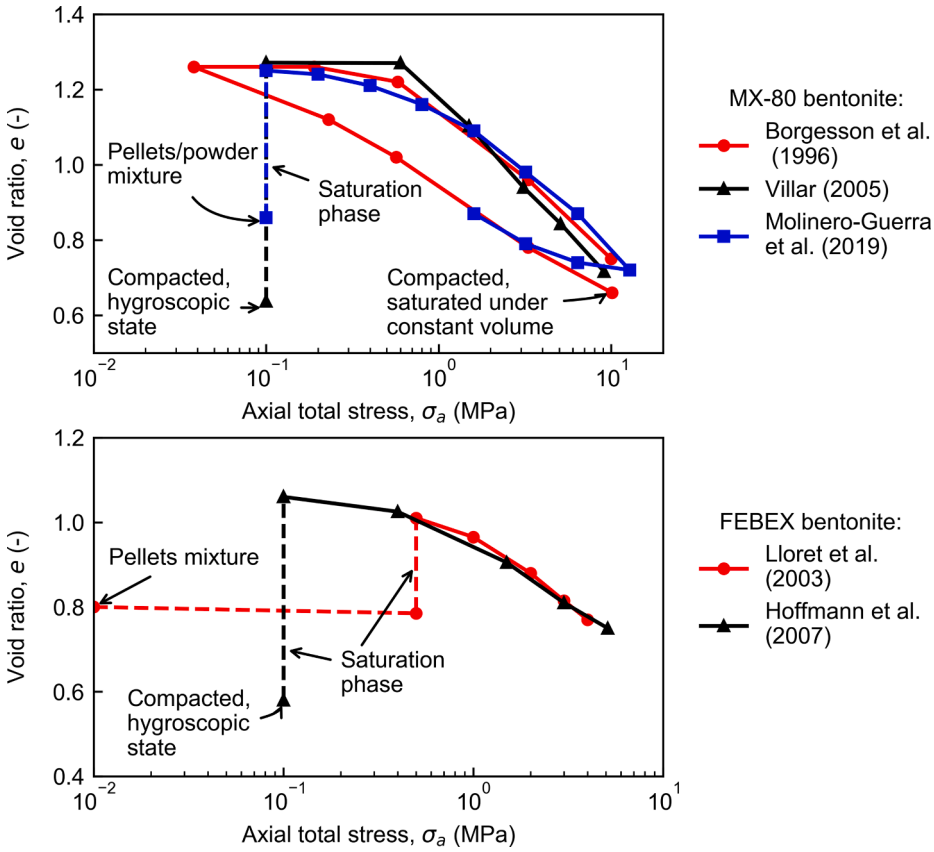

Fig. 2. Influence of initial compacted state and saturation path on compressibility and swelling of bentonite at saturated state. a) Oedometric compression on MX80 bentonite in block form (Börgesson et al., 1996; Villar, 2005) and pellets mixture (Molinero Guerra et al., 2019) after saturation. b) Oedometric compression on FEBEX bentonite in block form (Lloret et al., 2003) and pellets (Hoffmann et al., 2007) after saturation.

Saiyouri et al. (2004), Devineau et al. (2006) and Holmboe et al. (2012) found that the third layer of adsorbed water only developed when bentonite was confined on hydration.

Nevertheless, available data suggest that up to the bi-hydrated state, the adsorbed water can be approximated as a unique function of *RH*, regardless of the dry density or confinement conditions. In contrast, the development of the third layer (and eventually, the fourth layer) of the adsorbed water may be dependent on the available pore space. This observation is consistent with that of Romero and Vaunat (2000), who identified a unique WR behaviour of Boom clay at high suctions, regardless of the dry density. Accordingly, the capillary water and adsorbed water beyond the bi-hydrated state can be lumped together for modelling purposes. Although this is an approximation, it provides a fundamental division of pore water owing to the different structure and properties of the bi-hydrated state with respect to the third layer of adsorbed water.

2.2. *Influence of initial fabric on volumetric behaviour in saturated states*

Different compacted states of bentonite backfills, such as compacted blocks (Lloret et al., 2003), pellets of highly compacted bentonite (Hoffmann et al., 2007), well-graded mixtures of pellets (Seiphoori et al., 2014), and shot-clay bentonite (Ferrari et al., 2014), have been investigated. The role of the as-compacted fabric in soil behaviour in unsaturated states was reviewed and discussed by Alonso et al. (2013), who showed that collapse potential and compressibility are significantly dependent on the compacted state for a given soil, whereas, for low-activity soils, the slope of the Normal Compression Line (NCL) after saturation appears to be less sensitive to the initial as-compacted state. The aim of this section is to review the effects of the initial bentonite fabric on the volume change behaviour in saturated states.

Fig. 2 shows the results of oedometric tests on MX80 bentonite (Börgesson et al., 1996; Villar, 2005; Molinero Guerra et al., 2019) and FEBEX bentonite (Lloret et al., 2003; Hoffmann et al., 2007). These results include bentonite in a compacted form (Lloret et al., 2003; Villar, 2005; Börgesson et al. 1996), highly compacted pellets (Hoffmann et al., 2007), and pellet/powder mixtures (Molinero Guerra et al., 2019) saturated following different stress paths. After saturation, the tests consisted of loading or unloading–loading. Two main observations can be made. First, the swelling leads to fairly similar void ratio values for a specific stress state; second, the virgin compression line appears to be largely independent of the initial fabric and saturation path. In addition, the initial swelling for results obtained by Villar (2005) and Molinero Guerra et al. (2019) led to the same final void ratio at saturation, and the unloading phases in the results by Molinero Guerra et al., 2019 and Börgesson et al. (1996) showed the same unloading slope.

Gens et al. (2011) and Seiphoori (2014) concluded that the differences between the swelling pressure of bentonite pellet mixtures and compacted samples for a specific dry density are negligible. All these observations suggest that the macroscopic mechanical properties of bentonite tend to homogenise on saturation. Consequently, the volume change behaviour of bentonite in saturated states can be assumed to be independent of the initial compacted state.

3. Hydro-mechanical formulation

3.1. *Stress framework*

A Bishop stress form (Bishop, 1959) is adopted as the first constitutive stress variable using the degree of saturation as the pore-pressure averaging parameter:

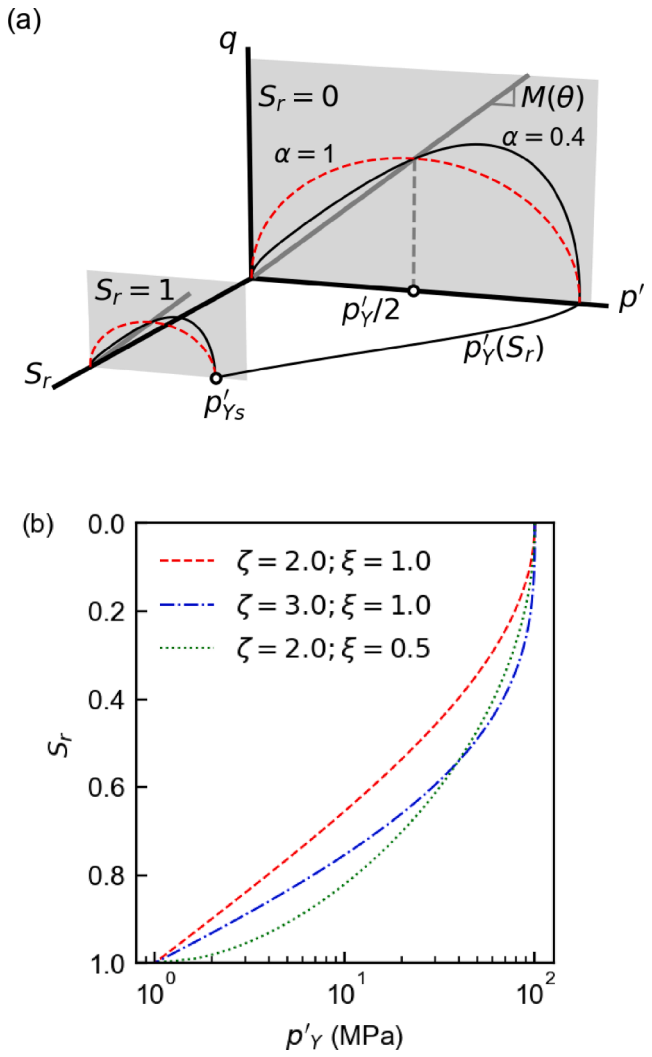

Fig. 3. a) Geometrical representation of the yield surface $f_Y = 0$ in $(p^{'}, q, S_r)$ space for $\alpha = 0.4$ and $\alpha = 1$. b) Influence of parameters ζ and ξ on the shape of the loading collapse curve with $r = 0.1$.

Table 1
Intrinsic material parameters of MX80 bentonite.

Mechanics (saturated state)		Water retention		Water transport	
κ	0.068	a	0.9 MPa^{-1}	$k_{f,0}(e_0 = 0.86)$	10^{-13} m/s
ν	0.35	b	1.5	*MKC*	6
λ_s	0.112	n_{VG}	1.8	*NKC*	5
$\phi^{'}_c = \phi^{'}_e$	11°	e^C_{ads}	0.55	τ	0.8
α	0.38				
$p^{'}_r$	1 Pa				

$$\boldsymbol{\sigma}' = \boldsymbol{\sigma} - [p_a - (p_a - p_w)S_r]\mathbf{I} = \boldsymbol{\sigma}^n + sS_r\mathbf{I} \quad (1)$$

where $\boldsymbol{\sigma}$ is the total stress tensor, p_w is the pore-water pressure, p_a is the pore-air pressure, $\boldsymbol{\sigma}^n = \boldsymbol{\sigma} - p_a\mathbf{I}$ is the net stress tensor, and s is the matric suction. In the following sections, $\boldsymbol{\sigma}'$ refers to the effective stress, in the sense that it is the variable linked to the elastic strains (Nuth and Laloui, 2008). For the considered applications, p_a was considered constant at $p_a = 0$.

Under high suction, high values of the effective stress can be obtained using Eq. (1). This can lead to the over-prediction of the shear strength and made some researchers disregard the contribution of either the water in the microstructure (Alonso et al., 2010, 2013; Rosone et al., 2016) or the adsorbed water (Zhou et al., 2018) to the equivalent pore pressure in the effective stress formulation. Although this approach is reasonable for low-activity soils, the same principle might not be directly applicable to bentonite because most adsorbed water in bentonite exists as interlayer water (Fig. 1). In a simplified manner, using the total degree of saturation in Eq. (1), it is recognised that interlayer water plays a critical role in the volume change under relatively high suction.

S_r is used in addition to Eq. (1) to express the evolution of compressibility and yield pressure with suction in formulating a complete model for unsaturated states. The advantages of formulating constitutive equations in the $(p^{'}, S_r, e)$ space for low-activity soils are reported by Zhou et al. (2012a; 2012b), which includes a natural transition between unsaturated and saturated states on compression. Because the air entry value is not explicitly required to define the

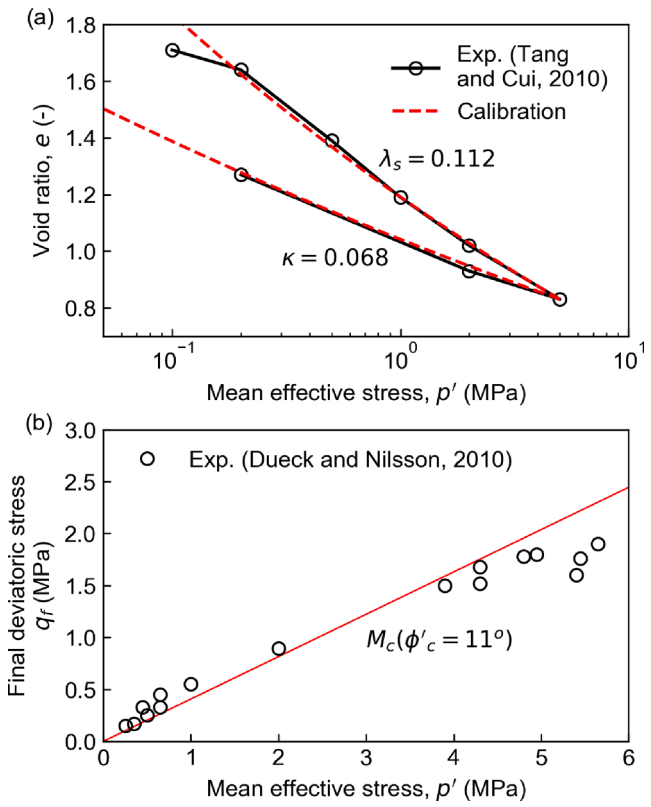

Fig. 4. Calibration of mechanical parameters for saturated MX-80 bentonite: (a) Calibration of κ and λ_s; (b) Calibration of $\phi^{'}_c$.

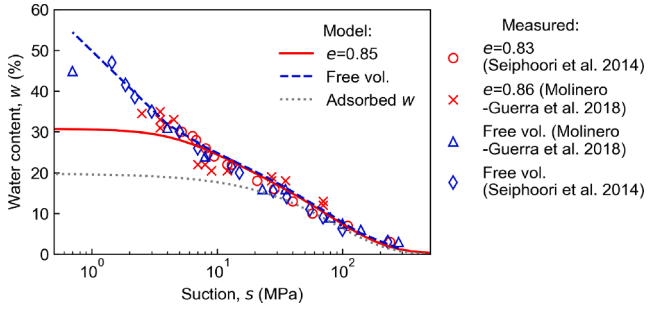

Fig. 5. Relationships between water retention of MX80 bentonite pellets mixture and experimental data obtained by Seiphoori et al. (2014) and Molinero-Guerra et al. (2018).

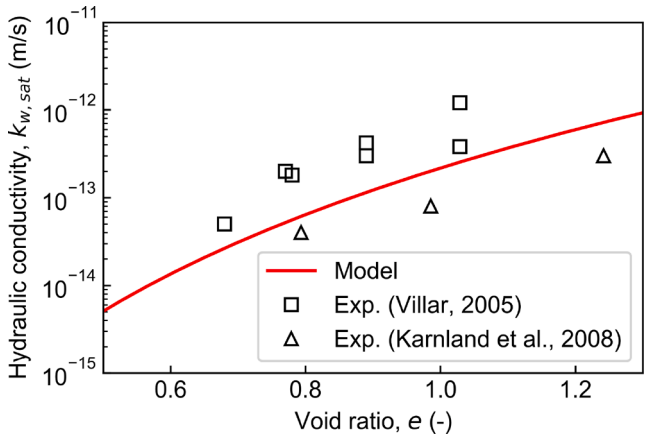

Fig. 6. Dependency of hydraulic conductivity on void ratio based on experimental data by Villar (2005) and Karnland et al. (2008).

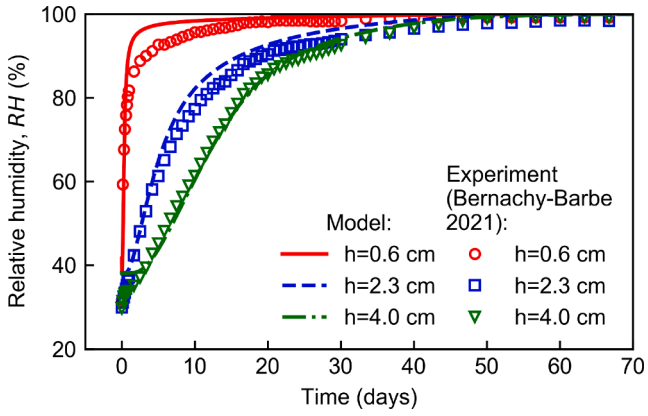

Fig. 8. Model calibration in terms of relative humidity compared to the experimental data obtained by Bernachy-Barbe (2021) for Test C1 (wetting at h = 0).

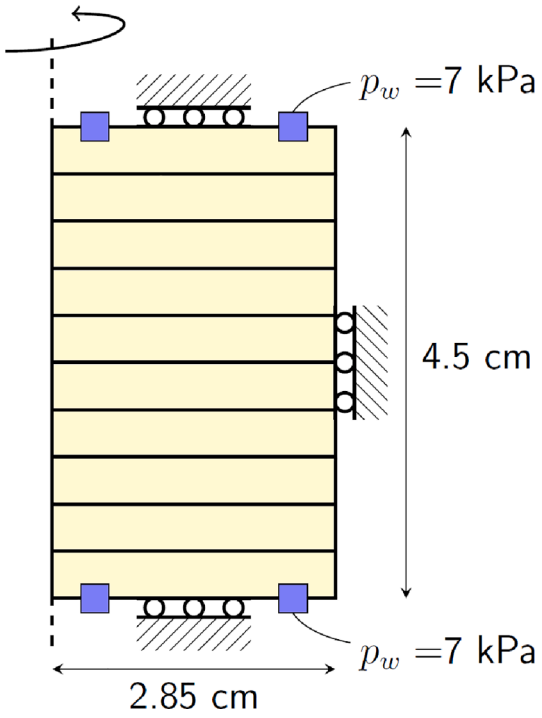

Fig. 7. Finite element discretisation and boundary conditions of test C2. Test C1 consisted on hydration from the bottom part only.

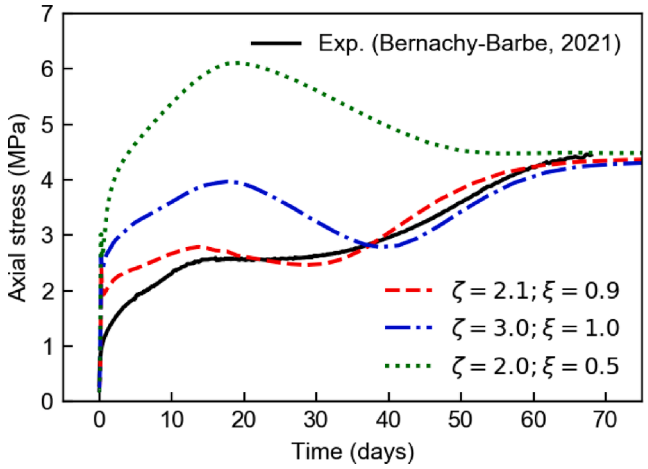

Fig. 9. Influence of parameters ζ and ξ on the swelling pressure development.

transition between saturated and unsaturated states, it represents an additional advantage for bentonites, as this parameter significantly evolves with the void ratio (Seiphoori et al., 2014).

3.2. Water retention model

For conciseness, the developments presented in this paper correspond to the main wetting paths, which is the focus of this study (hydration tests). Where experimental evidence is available, extensions can be expected to include hydraulic hysteresis.

Consistent with the analysis presented in Section 2, a WR model is established as a combination of an isotherm, describing the adsorption of the first two molecular water layers, and a capillarity-based model, which accounts for the free water (water beyond the bi-hydrated state). Such a conceptual WR model can be described by extending the framework presented by Revil and Lu (2013). Accordingly, the water ratio e_w (ratio of water volume to volume of solids) is divided into the free water ratio $e_{w,f}$ (volume of free water to volume of solids) and adsorbed water ratio $e_{w,a}$ (volume of adsorbed water to volume of solids):

$$e_w = e_{w,f} + e_{w,a} \tag{2}$$

The degree of saturation is obtained as $S_r = e_w/e$, where e is the void ratio. The development of the free water ratio $e_{w,f}$ is modelled using a modified van Genuchten expression (van Genuchten, 1980), assuming

Table 2
Parameters of pellet–powder mixture and block bentonite.

Parameter	Pellet mixture	Block
r	0.29	0.235
ζ	2.1	2.5
ξ	0.9	0.4
α_{kw}	4	2.9
m	0.65	1.0
Initial state		
e	0.85 (C1) 0.87 (C2)	0.68
s	130 MPa (C1) 110 MPa (C2)	110 MPa
$p_{Ys}^{\cdot}$	0.045 MPa (C1) 0.0278 MPa (C2)	0.89 MPa

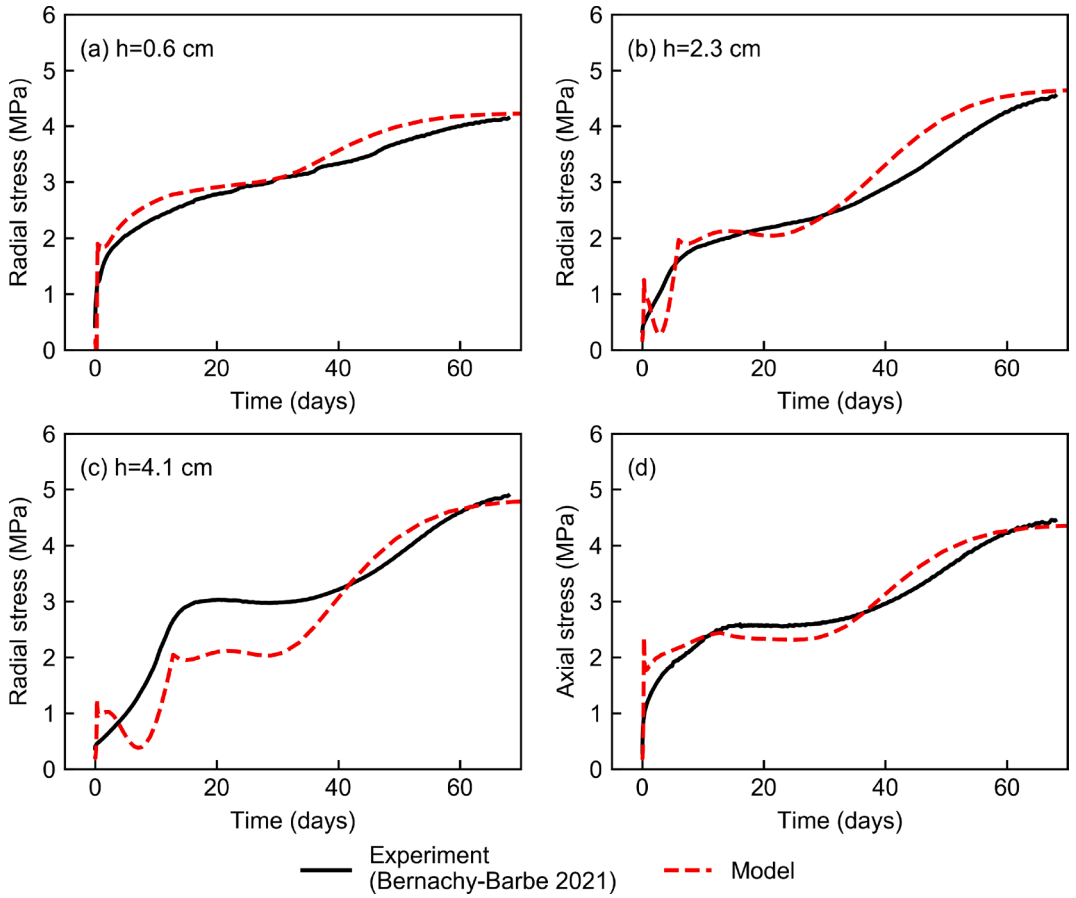

Fig. 10. Experimental and model results of Test C1 that consisted in wetting from the bottom (h = 0). Model results are presented in terms of radial stress at different heights: (a) h = 0.6 cm, (b) h = 2.3 cm, (c) h = 4.1 cm, and (d) axial stress. Experimental results from Bernachy-Barbe (2021).

that the interlayer space is always saturated:

$$e_{w,f} = \left(e - e_{w,a}\right)\left[1 + \left(\alpha_{VG} s\right)^{n_{VG}}\right]^{1/n_{VG}-1} \tag{3}$$

where n_{VG} depends on the pore network structure, and α_{VG} is related to the air entry value. Whereas Revil and Lu (2013) neglected the effect of volume change on the WR, this is considered here by adopting α_{VG} as a function of the void ratio not occupied by the adsorbed water, using the equation derived by Gallipoli et al. (2003b) and modified by Dieudonne et al. (2017):

$$\alpha_{VG} = a\left(e - e_{w,a}\right)^{b} \tag{4}$$

where a relates to the air entry value, and b is a material parameter that reflects the evolution of air entry value.

$e_{w,a}$ is a function of relative humidity, using the Freundlich isotherm (Freundlich, 1909):

$$e_{w,a} = e^{C}_{w,a}(RH)^{1/m} \tag{5}$$

where $e^{C}_{w,a}$ is the adsorption capacity, which corresponds to the maximum value of the adsorbed water ratio, which depends on the specific surface of the soil, and m is a parameter that mainly depends on the type of exchangeable cations. In Eq. (5), RH may be related to the suction s using Kelvin's law and expressed as follows:

$$e_{w,a} = e^{C}_{w,a}\left[\exp\left(-\frac{M_w}{\rho_w RT} s\right)\right]^{1/m} \tag{6}$$

where $R = 8.314$ J/mol K, M_w is the molar mass of water, ρ_w is the water density and T is the temperature. Other adsorption models could be used (e.g. Sedighi and Thomas, 2014; Dieudonne et al., 2017). In this work, Eq. (5) has been chosen based on the practical use of such expression, which only requires the definition of two parameters that can be found with common water retention tests.

Although the suction term in Eq. (6) refers to total suction, in this study the formulation was used for modelling cases in which hydration is performed with very low and constant salinity water, such that for a given suction and void ratio, osmotic suction can be considered constant. Thus, a unique suction term is used, and changes in material state due to osmotic suction are implicitly accounted for in s.

3.3. Stress–strain constitutive equations

According to the theory of elasto-plasticity, an explicit distinction between the elastic (reversible) and plastic (irreversible) strain increments is made:

$$\mathrm{d}\boldsymbol{\epsilon} = \mathrm{d}\boldsymbol{\epsilon}^{e} + \mathrm{d}\boldsymbol{\epsilon}^{p} \tag{7}$$

where $\boldsymbol{\epsilon}$ is the total strain tensor, and superscripts e, p denote elastic and plastic strains, respectively. The constitutive equations are expressed in terms of the stress invariants mean effective stress $p' = \mathrm{tr}(\boldsymbol{\sigma}')/3$, deviatoric stress $q = \sqrt{3}J$, and Lode's angle $\theta = \frac{1}{3}sin^{-1}\left(3\sqrt{3}\,det s/2J^3\right)$, where $\mathbf{s} = \sigma' - p'\mathbf{I}$, and $J = \sqrt{\mathrm{tr}(\mathbf{s}^2)/2}$. Similarly, the volumetric strain $\epsilon_v = \mathrm{tr}(\boldsymbol{\epsilon})$ and deviatoric strain $\epsilon_d = \sqrt{2\mathrm{tr}(\boldsymbol{\gamma}^2)/3}$ invariants are defined, where $\boldsymbol{\gamma} = \boldsymbol{\epsilon} - \epsilon_v\mathbf{I}/3$. The elastic strain increments are related to effective stress increments, as follows:

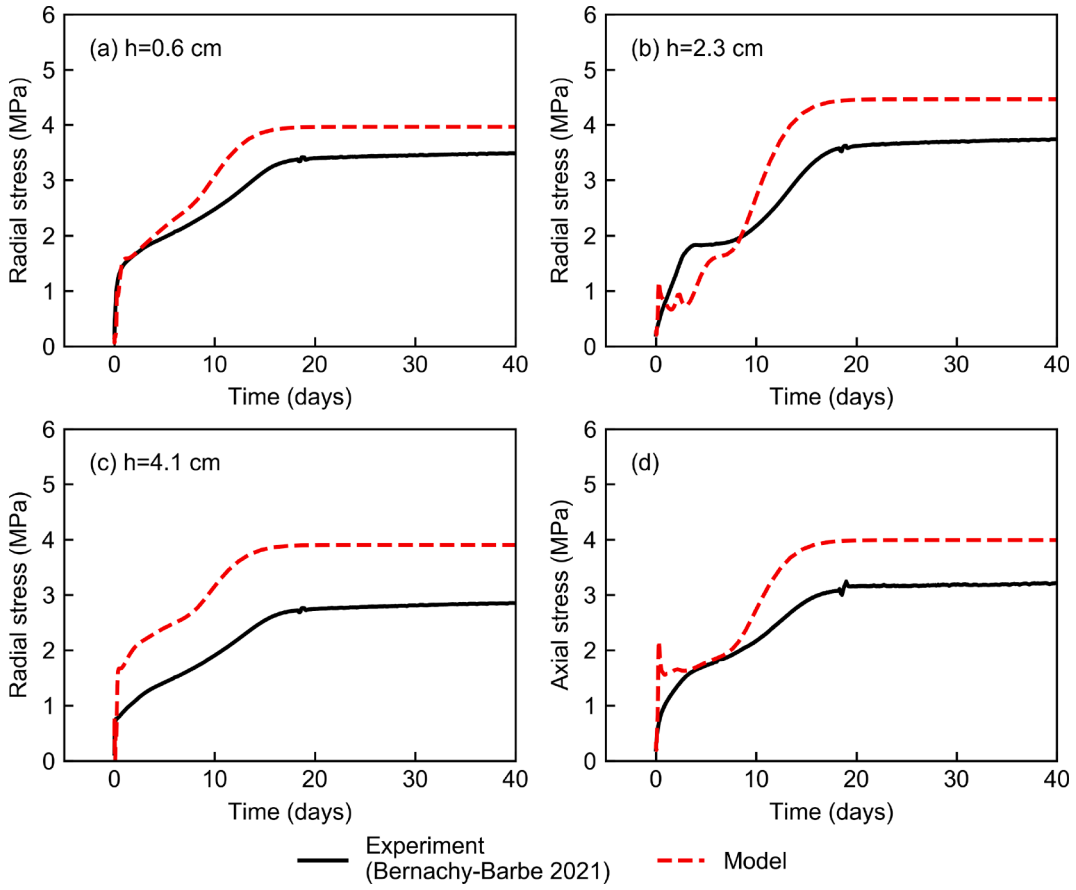

Fig. 11. Experimental and model results of Test C2, that consisted in wetting from bottom (h = 0) and top (h = 4.5 cm). Model results are presented in terms of radial stress at different heights: (a) h = 0.6 cm, (b) h = 2.3 cm, (c) h = 4.1 cm, and (d) axial stress. The experimental results were obtained by Bernachy-Barbe (2021).

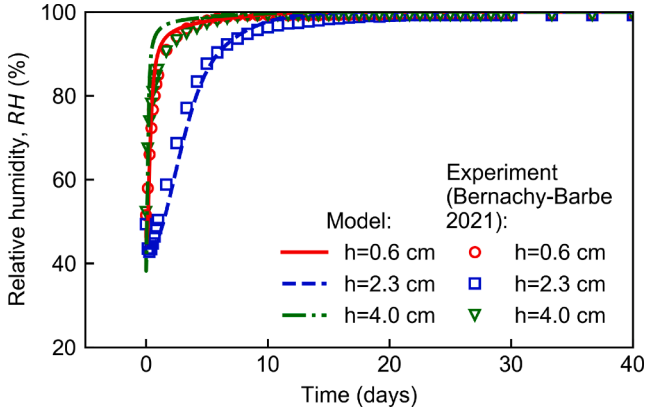

Fig. 12. Model results in terms of RH compared to experimental data obtained by Bernachy-Barbe (2021) obtained for Test C2 (wetting at h = 0 and h = 4.5 cm).

$$d\epsilon_v^e = \frac{p'}{\kappa} dp', \; d\epsilon_d^e = \frac{9(1-2\nu)}{2(1+\nu)} \frac{p'}{\kappa} dq \tag{8a,b}$$

where κ and ν are elastic material parameters.

The yield surface f_Y in the (p', q) plane is adopted from the study by Collins and Kelly (2002):

$$f_Y = q^2 - M^2 \left[\alpha + (1-\alpha)\left(\frac{2p'}{p'_Y}\right)\right]^2 (p'_Y - p')p' = 0 \tag{9}$$

where $M = M(\theta)$ is the critical stress ratio, α is a material parameter, and p'_Y corresponds to the yield pressure at the current S_r. The strength dependency on the stress path is established by expressing the critical stress ratio as a function of θ (van Eekelen, 1980; Vilarrasa et al., 2017):

$$M = a_L[1 - b_L \sin(3\theta)]^{-0.229} \tag{10}$$

where a_L and b_L are defined as:

$$a_L = \frac{M_c}{(1+b_L)^{-0.229}}, \quad b_L = \frac{\left(M_c/M_e\right)^{1/-0.229} - 1}{\left(M_c/M_e\right)^{1/-0.229} + 1}$$

In Eq. (11), $M_c = (6\sin\phi'_c)/(3 - \sin\phi'_c)$, $M_e = (6\sin\phi'_e)/(3 + \sin\phi'_e)$, and ϕ'_c and ϕ'_e are the shear strength angles for the compression and extension paths, respectively. As a first approximation, $\phi'_e = \phi'_c$ is considered acceptable for many clays (van Eekelen, 1980).

The direction of the plastic strain increments is determined following the flow rule derived by Collins and Kelly (2002):

$$\frac{d\epsilon_d^p}{d\epsilon_v^p} = \frac{q}{M^2(p' - p'_Y/2)\left[\alpha + (1-\alpha)\left(\frac{2p'}{p'_Y}\right)\right]^2} \tag{12}$$

Thus, α can be obtained by imposing that the oedometric compression along the virgin compression line satisfies the relationship, $K_0 = \sigma'_r/\sigma'_a = 1 - \sin(\phi'_c)$, where σ'_r and σ'_a are the radial and effective axial stresses, respectively (Alonso et al., 1990).

The yield pressure at saturated states p'_{Ys} evolves according to the hardening law:

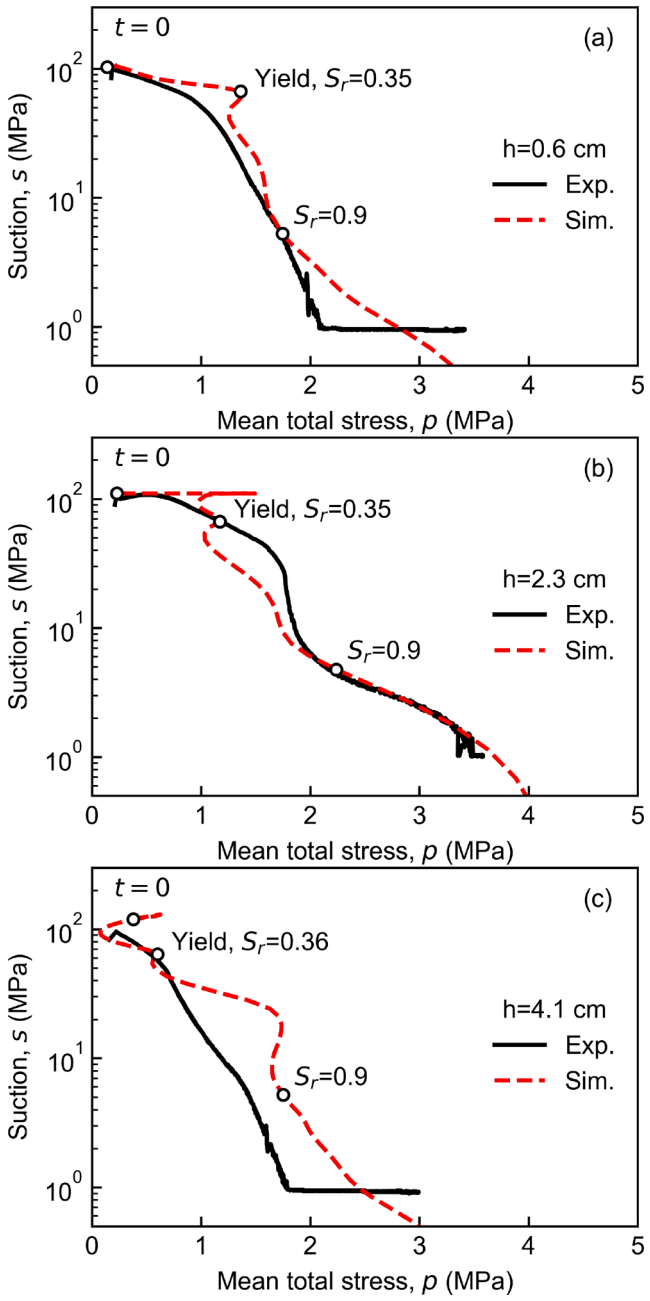

Fig. 13. Model and experimental results for mean total stress and suction of Test C2: (a) at h = 0.6 cm, (b) C2 at h = 2.3 cm, (c) C2 at h = 4.1 cm. The suction from the experiments was computed based on the *RH* reported by Bernachy-Barbe (2021).

$$\frac{\mathrm{d}p^{'}_{Ys}}{p^{'}_{Ys}} = \frac{\mathrm{d}\epsilon^{p}_{v}}{\lambda_s - \kappa} \tag{13}$$

where λ_s defines the elastoplastic compressibility for the saturated states. For unsaturated states, the dependency of the elastoplastic compressibility λ on S_r is not straightforward to determine as a result of the few experimental data on unsaturated compression of bentonite, at constant water content, available. Nevertheless, it can be indirectly estimated trough the simulation of swelling pressure tests, from which the following expression was found suitable:

$$\lambda = \lambda_s - r(\lambda_s - \kappa)\left(1 - S_r^{\zeta}\right)^{\xi} \tag{14}$$

where the parameter r $(0 < r < 1)$ expresses the maximum decrease in elastoplastic compressibility from the saturated to dry state ($S_r = 0$), and ζ and ξ are parameters that define the unsaturated compressibility evolution. Although these parameters are difficult to determine from direct measurements, it will be shown in Section 4.1 that they largely define the evolution of swelling pressure during hydration. Similar to Zhou et al. (2012b), the plastic volumetric strains of a soil yielding in variably saturated states are determined as:

$$\frac{\mathrm{d}p^{'}_{Y}}{p^{'}_{Y}} = \frac{\mathrm{d}\epsilon^{p}_{v}}{\lambda - \kappa} \tag{15}$$

By integrating Eqs. (13) and (15) and assuming that the resulting compression lines at different S_r values converge at a pressure determined using a material parameter $p^{'}_{r}$, the loading-collapse curve in the $(p^{'}, S_r)$ space is obtained:

$$\frac{p^{'}_{Y}}{p^{'}_{r}} = \left(\frac{p^{'}_{Ys}}{p^{'}_{r}}\right)^{\frac{\lambda_s - \kappa}{\lambda - \kappa}} \tag{16}$$

A similar expression was proposed by Alonso et al. (2013) although in terms of different constitutive variables. Different compressibility responses can be modelled with Eq. (16). For a given range of void ratio, if $p^{'}_{r}$ and r are chosen relatively low, it implies that compression lines at different S_r display similar slopes, whereas if $p^{'}_{r}$ and r are relatively high the different compression lines diverge significantly.

The yield surface in the $(p^{'}, q, S_r)$ space is depicted in Fig. 3a, which shows the effect of parameter α on the surface shape. Fig. 3b shows the influence of ζ and ξ on the loading collapse curve.

3.4. Transport equations

The constitutive model has been implemented in the finite element code LAGAMINE (Charlier, 1987; Collin et al., 2002), in order to perform numerical analysis of non-isothermal multiphase flow in deformable media. The water and vapour flow under isothermal conditions were considered for the presented cases. Water flow was modelled according to Darcy's law, assuming constant water viscosity, constant water density, and isotropic permeability:

$$\mathbf{q}_w = -\mathbf{I} k_f k_{rw} \mathbf{grad}(p_w + \rho_w g z) \tag{17}$$

where $\mathbf{q}_w$ is the water flux vector, k_f is the saturated hydraulic conductivity, k_{rw} is the relative permeability, g is the gravity and z the vertical coordinate. The relative permeability depends on the degree of saturation S_r following an exponential law:

$$k_{rw} = S_r^{\alpha_k} \tag{18}$$

where α_k is a material parameter. The deformation effect on hydraulic conductivity is reflected using a modified Kozeny–Carman equation:

$$k_f = k_{f,0} \frac{(1 - n_0)^{MKC}}{n_0^{NKC}} \frac{n^{NKC}}{(1 - n)^{MKC}} \tag{19}$$

where $k_{f,0}$ is the initial hydraulic conductivity for porosity n_0, n is the current porosity, and *MKC* and *NKC* are material parameters. Vapour is assumed to flow according to Fick's law in porous media:

$$\mathbf{i}_v = n(1 - S_r)\tau D \mathbf{grad}(\rho_v) \tag{20}$$

where $\mathbf{i}_v$ is the vapour flux, τ is the tortuosity, and $D = 2.363 \times 10^{-5}$ m^2/s (Philip and de Vries, 1957) is the diffusion coefficient. The gradient of the vapour density at a constant temperature is approximated as follows (Collin et al., 2002):

$$\mathbf{grad}(\rho_v) = -RH \frac{\rho_{v0} M_w}{\rho_w RT} \mathbf{grad}(s) \tag{21}$$

where ρ_{v0} is the saturated vapour density.

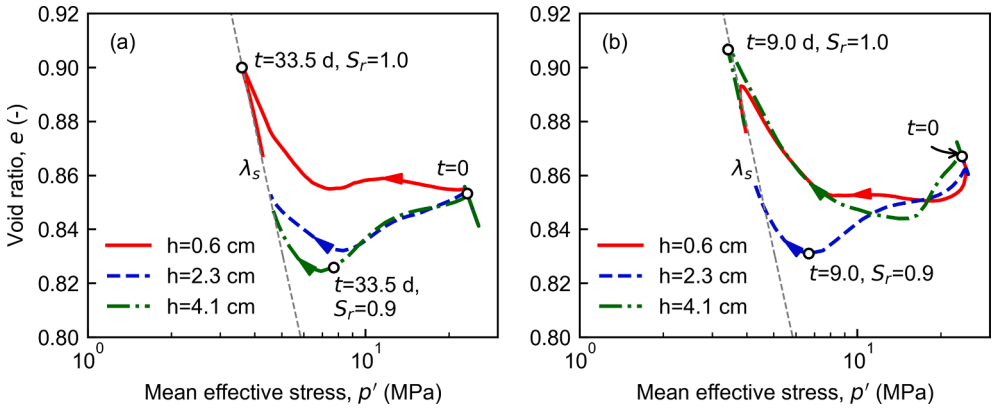

Fig. 14. Stress paths in plane $(p^{'}, e)$ for Tests (a) C1 and (b) C2.

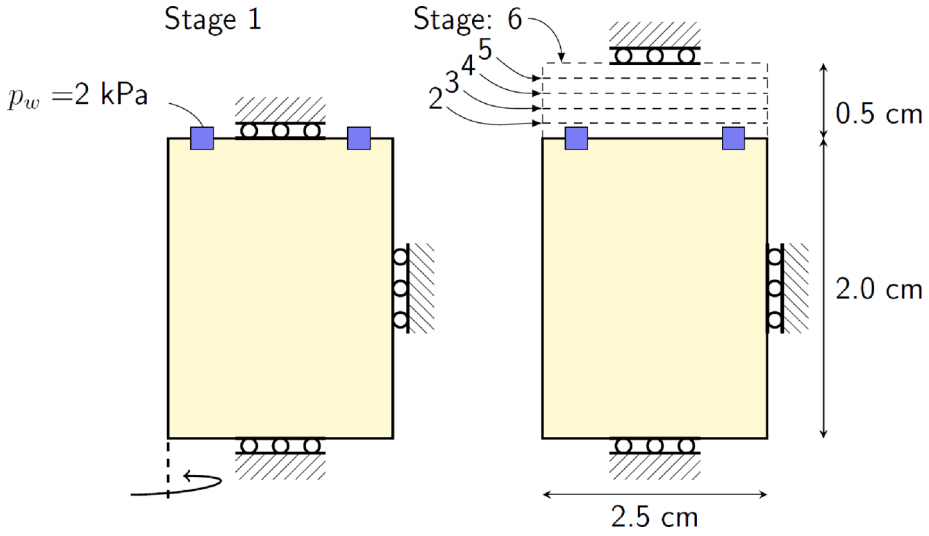

Fig. 15. Geometry, boundary conditions and stages of the gap filling tests reported by Dueck et al. (2011).

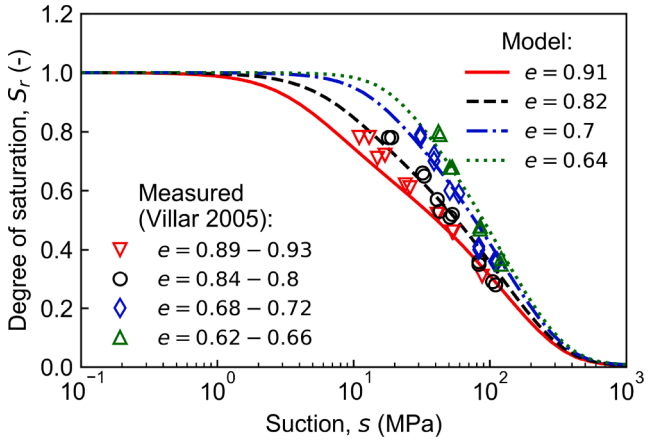

Fig. 16. Water retention model of MX-80 block bentonite calibrated against experimental data obtained by Villar (2005) at constant volume and various void ratios.

4. Analysis of swelling pressure tests

The hydro-mechanical formulation was used to model and analyse the behaviour of MX-80 bentonite, a material extensively tested over the last decades for its potential use as a backfill in geological repositories. The large amount of data obtained for this material behaviour could be used to calibrate the model and evaluate the predictive capabilities with different sets of laboratory experiments. All modelled tests involved hydration paths with distilled water and conducted at ambient temperatures under isothermal conditions.

Bernachy-Barbe (2021) performed a series of swelling pressure tests using local measurements of stress and *RH* and provided valuable data for the hydro-mechanical interpretation of swelling pressure. The tested material was a mixture of 50% mass of highly compacted MX-80 bentonite pellets (with an average dry density of 2 Mg/m^3) and 50% bentonite in powder form (with an average dry density of approximately 1.50 Mg/m^3), which corresponded to $e = 0.85$. The height and diameter of each specimen were 4.5 and 5.7 cm, respectively. Two tests are analysed in this section: Test C1, in which the mixture was hydrated from the bottom (corresponding to h = 0, where h is the height of the sample), and Test C2, in which the mixture was wetted from both sides. For modelling purposes, an equivalent homogeneous material under an axisymmetric condition was assumed.

As stated in Section 2.2, in this study the saturated state behaviour is assumed to be independent of the as-compacted state of the bentonite for the ranges of densities and stresses considered in geological repositories. To test this assumption, a single set of parameters describing the mechanical response when $S_r = 1$ was used for the MX80 bentonite in pellet, powder, and block forms (Table 1). The calibration of these parameters is shown in Fig. 4. $\kappa = 0.068$ and $\lambda_s = 0.112$ were defined based on isotropic compression and unloading at saturated states

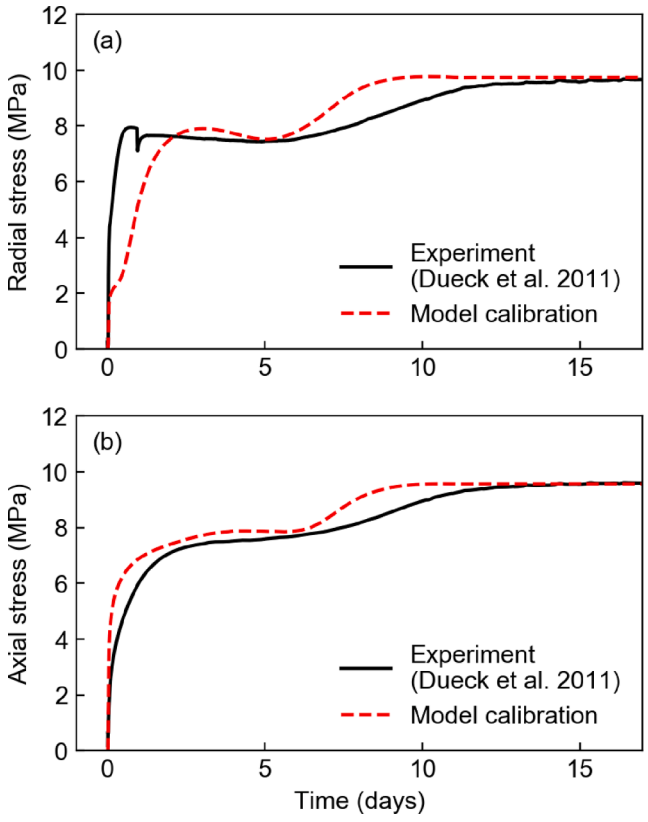

Fig. 17. Model calibration of the block bentonite behaviour under unsaturated states against swelling pressure test A01-10 results reported by Dueck et al. (2011): (a) results in terms of radial stress and (b) axial stress.

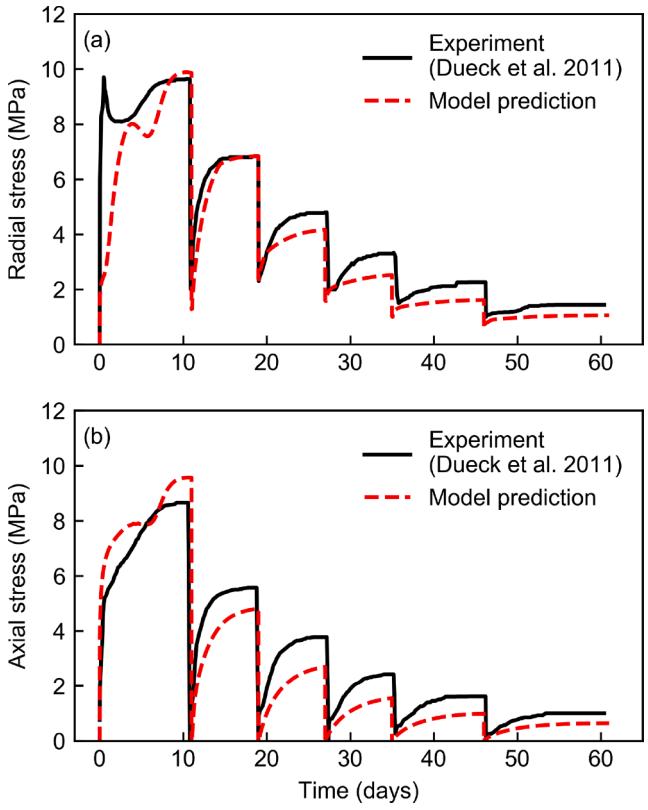

Fig. 18. Predicted response of the model against tests A01-3 and A01-12 reported by Dueck et al. (2011): (a) Test A01-3 radial stress, (b) axial stress.

reported by Tang and Cui (2010). Dueck and Nilsson (2010) obtained triaxial test results, from which $\phi_c^{'} = 11^{\circ}$ was derived from the slope of the critical state line. In the absence of specific tests, $\nu = 0.35$ was assumed. Based on these parameters, $K_0 = 1 - \sin\phi_c^{'}$ for oedometric saturated compression was obtained when $\alpha = 0.38$.

The water retention behaviour of the pellet/powder mixtures was calibrated using the data shown in Fig. 5, obtained by Molinero Guerra et al. (2019) for pellet/powder mixtures (80/20 mass proportion), and Seiphoori et al. (2014) for a granular mixture of bentonite pellets. Both constant and free volume conditions under hydration were considered for calibration. The calibration started with the adsorbed water parameters, as these do not depend on void ratio. The water content at which WR curves at different void ratios converge can be used to derive $e_{w,a}^{C}$ and m is used to fit the curve at higher suctions. Afterwards parameters a, b and n_{VG}, defining the free water behaviour were established. A satisfactory fit for both constant volume and free volume conditions was obtained using the water retention model. The computed adsorbed water content is also shown in Fig. 5 in order to visualise its contribution to the high suction range. Fig. 6 shows the calibration of saturated hydraulic conductivity as a function of e (Eq. (19)) using the data presented by Villar (2005) and Karnland et al. (2008). All these parameters are reported in Table 1.

Tests C1 and C2 were modelled as a boundary value problem considering an axisymmetric one-dimensional column. The domain was discretised into 10 *iso*-parametric finite elements, each with eight nodes and four integration points. Further discretisation did not influence the results. The finite element mesh and boundary conditions are represented in Fig. 7. Test C1, which comprised hydration at h = 0, was back-analysed to determine first the hydraulic conductivity in unsaturated states, i.e. α_k (Eq. (18)), and afterwards the parameters r, ζ, and ξ of the mixture.

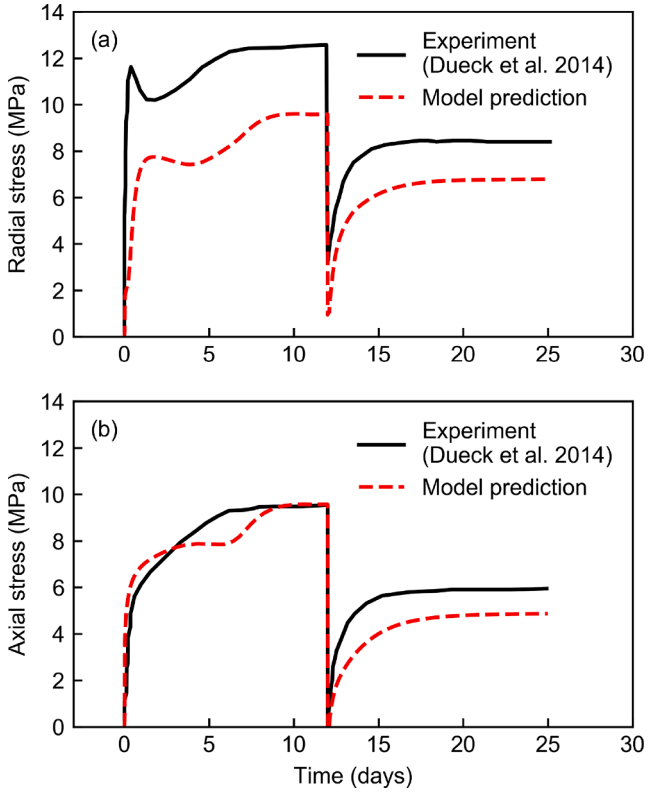

Fig. 19. Predicted response of the model against tests A01-12 reported by Dueck et al. (2014): (a) radial stress, (b) axial stress.

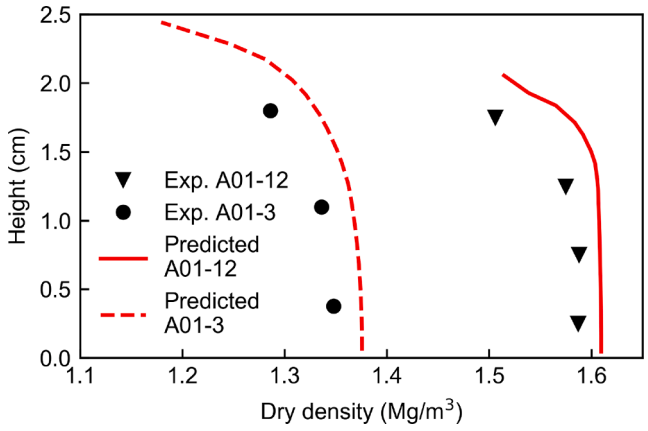

Fig. 20. Final distribution of dry density predicted by the model compared to experimental values reported by Dueck et al. (2011, 2014).

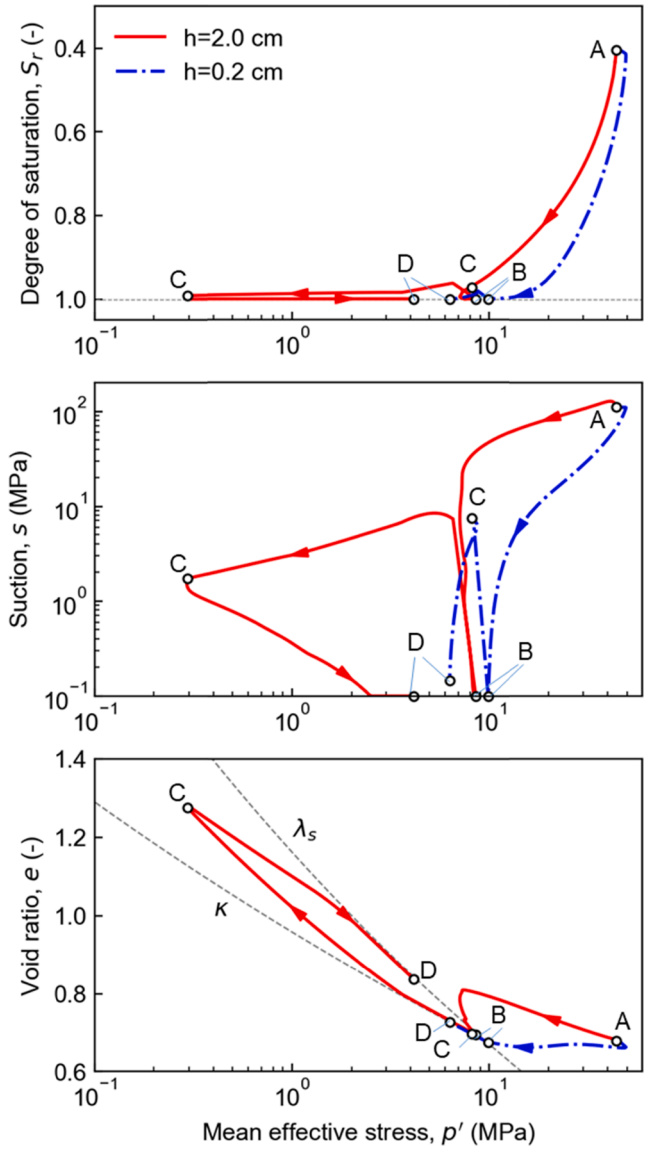

Fig. 21. Stress paths computed for Test A01-12 (saturation-unloading-swelling-swelling pressure) in space $(p^{\cdot}, S_r, s, e)$. The heights of the two points (h = 2 cm and 0.2 cm) indicate the initial state. The sample was hydrated at the top (initially at h = 2 cm).

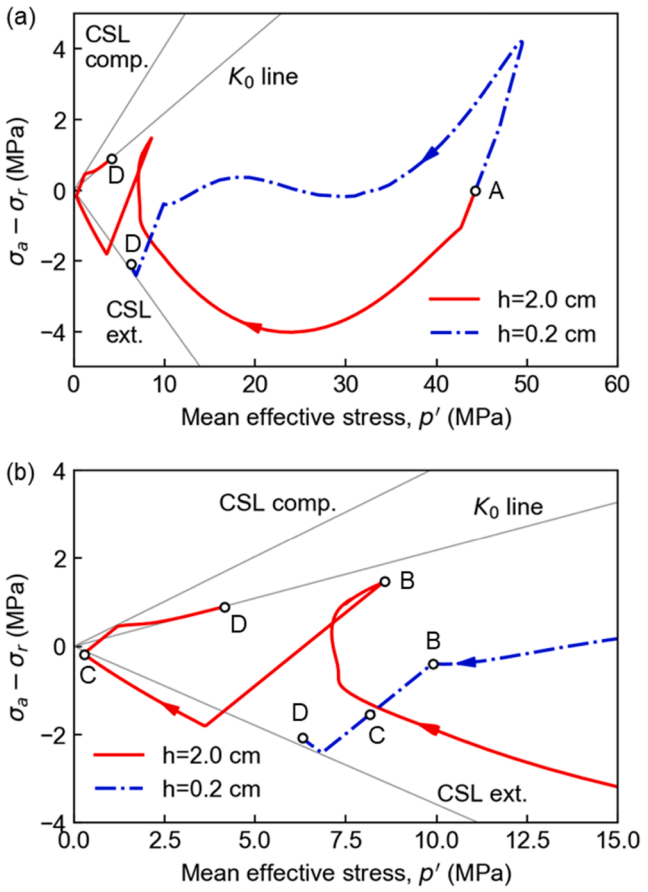

Fig. 22. (a) Stress paths computed for Test A01-12 (saturation-unloading-swelling-swelling pressure) in the space $(p^{\cdot}, \sigma_a - \sigma_r)$. (b) Zoom into paths after saturation. The heights of the two points (h = 2 and 0.2 cm) refer to the initial state. The sample was hydrated at the top (initially at h = 2 cm).

The estimated initial dry density in test C1 was 1.50 Mg/m^3 (e = 0.85), corresponding to an initial $p^{\cdot}_{Ys} = 0.045$ that located the normal compression line according to the results shown in Fig. 4(a). The initial water content was estimated to be w = 6.5%, which corresponded to an initial suction of 130 MPa according to the calibrated WR model. The relative humidity measurements were used to calibrate α_k = 4. The fit obtained is shown in Fig. 8.

Fig. 9 shows the influence of the parameters ζ and ξ on the development of swelling pressure. It can be observed that the unsaturated compressibility, or alternatively, the shape of the loading collapse curve controls the evolution of swelling pressure during hydration. Either a peak in swelling pressure higher than the final pressure (Imbert and Villar, 2006) or a progressive increase, as in the present case, can be represented. It can be noted that once saturation is reached, the same swelling pressure is obtained at roughly the same time in all cases. As it will be shown, the value at equilibrium is largely determined by the NCL that was calibrated independently. All parameters calibrated that depend on the initial state of the material are reported in Table 2.

The results are shown in Fig. 10 in terms of the average radial stresses at each height. Some oscillations at certain locations were obtained during the initial hydration due to the formulation of the effective stress (Eq. (1)) that are further discussed afterwards (Test C2) in terms of (p,s). At low values of S_r this formulation might not be accurate due, in part, to the initial heterogeneity of the mixtures. This heterogeneity implies that water may not be evenly distributed nor continuous across the pore space in the sample. Nevertheless, the practical use of Eq. (1) and its good performance at higher saturation compensated these limitations for the purposes of this study.

The set of parameters used to simulate Test C1 was applied to model Test C2. Test C2 consisted of the same pellet–powder mixture with a slightly lower dry density of an average value of 1.49 Mg/m^3 ($e = 0.87$), and the mixture was wetted from both ends (h = 0 and h = 4.5 cm as shown in Fig. 7). The initial water content was estimated to be $w =$ 6.8%, corresponding to an initial suction of 110 MPa according to the water retention model (Fig. 5). Fig. 11 shows the results in terms of stresses, including the experimental values for each height and the axial measurements. The predicted trend of the swelling pressure was very similar to the measured trend. Although the magnitude at equilibrium was overestimated, it remained within the experimental uncertainty in terms of dry density-swelling pressure (Bernachy-Barbe, 2021). The time at which such an equilibrium is reached was well predicted. The predicted *RH* evolution is shown in Fig. 12, which was consistent with the measurements, except for the deviation at the top zone that could have resulted from the model idealisation of an initially homogeneous material, leading to an exactly symmetric water uptake.

The computed stress paths at each height are shown in Fig. 13, in addition to the measured mean total stress and total suction which enable to interpret the tests according to the model. Since total suction was computed from the measured *RH* and *T*, suction values lower than 1 MPa were not obtained. In the early stages, the zones far from the hydration boundaries (Fig. 13b) were subjected to an increase in the total stress at constant suction, owing to the swelling of the bentonite close to the water intake. As the suction started to decrease, the total stress evolution depended on both the axial stress (developed by the global sample) and the decrease in sS_r that was locally compensated for to ensure null radial strains (Eq. 8) leading to high non-linear response (as observed also in Fig. 10). On yielding, at approximately $S_r = 0.35$, the swelling pressure remained almost constant despite the decrease in sS_r, owing to the compensation of elastic strains with plastic strains. As the bentonite approached the saturated state at approximately $S_r = 0.9$, the increase in swelling pressure depended on the saturation state of the adjacent zones. For instance, the zones that were wetted first did not experience a significant increase in swelling pressure; instead, they experienced swelling under low external stress. In contrast, the zones wetted in the late stages were subjected to external pressure applied by the neighbouring zones and, having limited swelling capacity, they developed higher swelling pressure than zones wetted in the early stages.

The simulated response as full saturation was approached is better represented in the space $(\log p', e)$, as shown in Fig. 14, because of local volume changes. A high initial p' corresponded to the product sS_r. The initial elastic response can be well identified, as all the points followed a unique line in the semi-logarithmic plane, defined by κ. As wetting continued and yielding occurred, the elasto-plastic response resulted in a wetting-collapse of different magnitudes, depending on the external stress on wetting. Subsequently, the swelling was obtained close to saturation, and when the bentonite close to the water uptake (h = 0.5 cm in Fig. 14a and h = 0.5 and h = 4.1 cm in Fig. 14b) was saturated, it was compressed by the inner bentonite that swelled as it approached saturation (after t = 33.5 and 9 days in Tests C1 and C2, respectively). The state at equilibrium appeared to be defined by the NCL (λ_s-line) that was independently calibrated against saturated compacted bentonite (Fig. 4). Given that the NCL is an exponential relationship between void ratio and mean effective stress, it might explain why the final swelling pressure was over predicted by the model. Indeed, small variations of dry density during the experimental testing (Bernachy-Barbe, 2021) not accounted in the simulation, might lead to some variations of swelling pressure.

5) Swelling potential of saturated bentonite

In addition to the intrinsic hydro-mechanical coupling, one of the main advantages argued by Nuth and Laloui (2008) on the use of the generalised effective stress framework was its efficiency in dealing with the transitions between unsaturated and saturated states. The interest in this feature in bentonite modelling was examined by analysing one of the tests performed by Dueck et al. (2011) on MX80 bentonite at an initial-state dry density of 1.65 Mg/m^3 with a water content of 10%. The aim was to assess the bentonite capability to seal eventual technological gaps in a repository after reaching full saturation. A schematic representation of the evolving boundary conditions is shown in Fig. 15. During the entire test hydration was imposed trough a constant water pressure on the upper side. After an initial phase of saturation under constant volume conditions (stage 1), the material was axially unloaded and allowed to swell up to a specific height under constant water pressure. Once the established height was reached, the swelling pressure resulting from the continuous water intake was measured. Both radial (σ_r) and axial (σ_a) stresses were measured.

Two tests, A0112 and A013 are analysed in this section. They comprise respectively two (test A0112) and five (test A013) cycles of unloading (swelling) and reloading (swelling pressure). Apart from the stress path complexity, the tests allowed for evaluating the consistency between the swelling strains, swelling pressure, and dry density profiles (obtained after dismantling) predicted by the model. The initial height of the tested specimens was 2.0 cm. For each swelling cycle the heigh increased 0.1 cm, such that at the end of the test the samples had a height of 2.1 cm (test A0112) and 2.5 cm (test A013).

As in the simulations presented in Section 4, the test was modelled as a boundary value problem using an axisymmetric column discretised into 10 eight-node *iso*-parametric finite elements, each with four integration points. All the mechanical parameters defining the saturated state behaviour were the same used for the previous tests on pellets mixtures (Table 1). The parameters that differ from those used in the pellets/powder mixture are reported in Table 2. The WR model for the MX-80 bentonite compacted in a block form was calibrated as shown in Fig. 16, against the experimental data reported by Villar (2005) for a constant volume at different void ratios. It was found that only the parameter m had to be changed with respect to the pellets mixture in order to fit the water retention behaviour of the blocks. The initial water content of $w = 10\%$ corresponds to an initial suction of 90 MPa according to the WR model (Fig. 16). The saturation phase (swelling pressure) of Test A0110 (Fig. 17) was used to calibrate the unsaturated permeability, adjusting α_k. The same test was used to calibrate the parameters r, ζ, and ξ for the high-density block. The fit obtained with the model is shown in Fig. 17.

The model predictions for tests A01-3 and A01-12 can be compared with the experimental results in Fig. 18 (A01-3) and Fig. 19 (A01-12). Overall a reasonable replication of the experimental results was achieved. The results from the different tests, (which started from the same initial conditions) also put into perspective the quantitative discrepancies between the model and the experiments, as the numerical discrepancies are in the order of magnitude of the experimental uncertainties. Fig. 20 shows the measured values of the dry density measured after the dismantling of the tests, in addition to the dry density profile predicted using the model. Although the dismantling operation involved the unconfinement of the samples, which decreased the overall dry density, the profiles of predicted dry density showed a similar gradient for both stages.

In order to highlight the convenience of the stress framework in reproducing the tests, the stress paths of the upper and lowest integration points are shown in Fig. 21 in the planes (s, S_r, e, p'). After the sample reached the saturated state (B), it was axially unloaded, inducing a suction increase because of the low permeability of the bentonite. Since the material was continuously hydrated from the top, the suction progressively reduced, and the sample swelled until it reached the height imposed by the piston (C). Subsequently, the volume was constrained again, and the upper element compressed as the suction on the lower elements decreased continuously, inducing a total stress increase until the pore water pressure (D) stabilised. This sequence was identical in subsequent cycles, although lower stress was generated as the overall dry density decreased.

The response during unloading (BC) followed the purely elastic regime only for a limited range of stress, after which the slope increased. This response was similar to that observed in the tests depicted in Fig. 2, in which the slope during swelling was somewhat similar to that during compression. The mechanism of the model that generated this response originated from the stress path in the plane $(p^{'}, \sigma_a - \sigma_r)$ shown in Fig. 22. Releasing the axial stress led to a high differential stress, owing to the existing radial confinement. Because of the relatively low shear strength angle, the yield surface in $(p^{'}, q)$ was reached during one-dimensional swelling, and subsequent swelling was elastoplastic. In both stages the stress state equilibrates at the NCL, which was established independent of these tests (Fig. 4), supporting again (in view of the consistency between final stress and dry density) the assumption of a unique saturated NCL for predictive purposes.

5. Conclusion

One of the main differences between bentonites and low-activity clays is the water adsorption in the interlayer spaces between smectite platelets. Interlayer water induces a unique hydraulic and volume change behaviour in bentonite. Although the interpretation of bentonite has been mainly focused on the influence of microstructure evolution, few analyses have considered the direct dependence of mechanical response on the actual degree of saturation. In this study, the behaviour of compacted bentonites during hydration was directly related to the water retention behaviour to evaluate the hydro-mechanical response.

X-ray diffraction results of bentonite at different dry densities and confining conditions suggest two water retention trends as a function of *RH*: water in the first two adsorbed layers (bi-hydrated state) and free water, which for convenience, also includes adsorbed water beyond the bi-hydrated state. Adsorption was modelled using an isotherm, which is independent of the void ratio, based on the observation that the development of the bi-hydrated state is practically independent of volume constraints. Conversely, a dependency on the void ratio was adopted for the free water retention mechanism. A literature survey of oedometric tests suggests that the volumetric behaviour of bentonite after saturation is largely independent of the initial fabric of the material and the saturation path. Thus, the behaviour in saturated states can be described using a single set of parameters.

A water retention and constitutive model have been presented based on current frameworks for low activity soils, extended in agreement with the interpretation. The hydro-mechanical coupling allows the water retention model to evolve consistently with density and the mechanical model to recover the saturated state properties at evolving air entry values. The equations have been implemented in a finite element code and laboratory tests on MX80 bentonite were simulated to gain further insight into bentonite behaviour during hydration. The parameters at the saturated states were first determined from basic laboratory tests. After the saturated state behaviour was defined, two sets of laboratory results for the response of bentonite during hydration were simulated. The first application involved two swelling pressure tests on pellet–bentonite mixtures monitored extensively, including radial stress and *RH* at various distances from the wetting front. All measurements were replicated consistently, including the time at which they reached saturation. The second application showed the ability of the coupled approach to simulate the swelling and swelling pressure in saturated states based on the high negative pore-water pressures. The numerical simulations supported the hypothesis that MX80 bentonite compacted in different forms tends to display a rather unique NCL after saturation.

CRediT authorship contribution statement

Jose A. Bosch: Investigation, Formal analysis, Writing – original draft. **Alessio Ferrari:** Supervision, Writing – review & editing. **Lyesse Laloui:** Supervision, Writing – review & editing.

Declaration of Competing Interest

The authors declare that they have no known competing financial interests or personal relationships that could have appeared to influence the work reported in this paper.

Acknowledgements

This work has received funding from the Euratom research and training programme 2014–2018 under grant agreement No 745942. The research group led by Prof. R. Charlier and Prof. F. Collin at the University of Liège is acknowledged for providing their software LAGAMINE and guidance on implementing the constitutive model. The authors also thank F. Bernachy-Barbe from CEA (France) for sharing experimental data and Etienne Cassini for insightful discussions.

References

Alonso, E.E., Gens, A., Josa, A., 1990. A constitutive model for partially saturated soils. Géotechnique 40 (3), 405–430.
Alonso, E.E., Vaunat, J., Gens, A., 1999. Modelling the mechanical behaviour of expansive clays. Eng. Geol. 54 (1-2), 173–183.
ALONSO, E.E., PEREIRA, J.-M., VAUNAT, J., OLIVELLA, S., 2010. A microstructurally based effective stress for unsaturated soils. Géotechnique 60 (12), 913–925.
ALONSO, E.E., PINYOL, N.M., GENS, A., 2013. Compacted soil behaviour: initial state, structure and constitutive modelling. Géotechnique 63 (6), 463–478.
Bernachy-Barbe, F., 2021. Homogenization of bentonite upon saturation: Density and pressure fields. Appl. Clay Sci. 209, 106122. https://doi.org/10.1016/j.clay.2021.106122.
Bestel, M., 2014. Water–montmorillonite systems: Neutron scattering and tracer through diffusion studies. Ph. D. dissertation. Universität Bern.
Bishop, A.W., 1959. The effective stress principle. *Teknisk Ukeblad* 39, 859–863.
Börgesson, L., Karnland, O., Johannesson, L.-E., 1996. Modelling of the physical behaviour of clay barriers close to water saturation. Eng. Geol. 41 (1-4), 127–144.
Charlier, R., 1987. Approche unifiée de quelques problèmes non linéaires de mécanique des milieux continus par la méthode des éléments finis. PhD Thesis. University of Liège, Belgium.
Collin, F., Li, X.L., Radu, J.P., Charlier, R., 2002. Thermo-hydro-mechanical coupling in clay barriers. Eng. Geol. 64 (2-3), 179–193.
Collins, I.F., Kelly, P.A., 2002. A thermomechanical analysis of a family of soil models. Geotechnique 52 (7), 507–518.
Vecchia, G.D., Jommi, C., Romero, E., 2013. A fully coupled elastic–plastic hydromechanical model for compacted soils accounting for clay activity. Int. J. Numer. Anal. Meth. Geomech. 37 (5), 503–535.
Devineau, K., Bihannic, I., Michot, L., Villiéras, F., Masrouri, F., Cuisinier, O., Fragneto, G., Michau, N., 2006. In situ neutron diffraction analysis of the influence of geometric confinement on crystalline swelling of montmorillonite. Appl. Clay Sci. 31 (1-2), 76–84.
Dieudonne, A.-C., Della Vecchia, G., Charlier, R., 2017. Water retention model for compacted bentonites. Can. Geotech. J. 54 (7), 915–925.
Dueck, A., Nilsson, U., 2010. Thermo-Hydro-Mechanical properties of MX-80. Results from advanced laboratory tests No. SKB-TR-10-55.
Dueck, A., Goudarzi, R., & Börgesson, L. (2011). Buffer homogenisation, status report (No. SKB-TR–12-02). SKB technical report.
Dueck, A., Goudarzi, R., & Börgesson, L. (2014). Buffer homogenisation, status report 2 (No. SKB-TR–14-25). SKB technical report.
Ferrari, A., Seiphoori, A., Rüedi, J., Laloui, L., 2014. Shot-clay MX-80 bentonite: An assessment of the hydro-mechanical behaviour. Eng. Geol. 173, 10–18.
François, B., Laloui, L., 2008. ACMEG-TS: A constitutive model for unsaturated soils under non-isothermal conditions. Int. J. Numer. Anal. Meth. Geomech. 32 (16), 1955–1988.
Freundlich, H., 1909. Kapillarchemie, eine Darstellung der Chemie der Kolloide und verwandter Gebiete. akademische Verlagsgesellschaft.
Gallipoli, D., Gens, A., Sharma, R., Vaunat, J., 2003a. An elasto-plastic model for unsaturated soil incorporating the effects of suction and degree of saturation on mechanical behaviour. Géotechnique. 53 (1), 123–135.
Gallipoli, D., Wheeler, S.J., Karstunen, M., 2003b. Modelling the variation of degree of saturation in a deformable unsaturated soil. Géotechnique. 53 (1), 105–112.
GENS, A., 2010. Soil-environment interactions in geotechnical engineering. Géotechnique 60 (1), 3–74.
Gens, A., Alonso, E.E., 1992. A framework for the behaviour of unsaturated expansive clays. Can. Geotech. J. 29 (6), 1013–1032.
GENS, A., VALLEJáN, B., SáNCHEZ, M., IMBERT, C., VILLAR, M.V., VAN GEET, M., 2011. Hydromechanical behaviour of a heterogeneous compacted soil: experimental observations and modelling. Géotechnique 61 (5), 367–386.
Hoffmann, C., Alonso, E.E., Romero, E., 2007. Hydro-mechanical behaviour of bentonite pellet mixtures. *Phys. Chem. Earth.*, Parts A/B/C 32 (8-14), 832–849.
Holmboe, M., Wold, S., Jonsson, M., 2012. Porosity investigation of compacted bentonite using XRD profile modeling. J. Contam. Hydrol. 128 (1-4), 19–32.
Houlsby, G.T., 1997. The work input to an unsaturated granular material. Géotechnique 47 (1), 193–196.

Imbert, C., Villar, M.V., 2006. Hydro-mechanical response of a bentonite pellets/powder mixture upon infiltration. Appl. Clay Sci. 32 (3-4), 197–209.
Jommi, C., 2000. Remarks on the constitutive modelling of unsaturated soils. Experimental evidence and theoretical approaches in unsaturated soils 139–153.
Karnland, O., Nilsson, U., Weber, H., Wersin, P., 2008. Sealing ability of Wyoming bentonite pellets foreseen as buffer material–laboratory results. Physics and Chemistry of the Earth, Parts A/B/C 33, S472–S475.
Lloret, A., Villar, M.V., Sánchez, M., Gens, A., Pintado, X., Alonso, E.E., 2003. Mechanical behaviour of heavily compacted bentonite under high suction changes. Géotechnique 53 (1), 27–40.
Low, P.F., 1980. The Swelling of Clay: II. Montmorillonites 1. *Soil science society of.* America journal 44 (4), 667–676.
Mašín, D., 2013. Double structure hydromechanical coupling formalism and a model for unsaturated expansive clays. Eng. Geol. 165, 73–88.
Mokni, N., Molinero Guerra, A., Cui, Y.-J., Delage, P., Aimedieu, P., Bornert, M., Tang, A. M., 2020. Modelling the long-term hydro-mechanical behaviour of a bentonite pellet/powder mixture with consideration of initial structural heterogeneities. Géotechnique 70 (7), 563–580.
Molinero Guerra, A., Cui, Y.-J., He, Y., Delage, P., Mokni, N., Tang, A.M., Aimedieu, P., Bornert, M., Bernier, F., 2019. Characterization of water retention, compressibility and swelling properties of a pellet/powder bentonite mixture. Eng. Geol. 248, 14–21.
Navarro, V., Asensio, L., Gharbieh, H., De la Morena, G., Pulkkanen, V.-M., 2020. A triple porosity hydro-mechanical model for MX-80 bentonite pellet mixtures. Eng. Geol. 265, 105311. https://doi.org/10.1016/j.enggeo.2019.105311.
Nuth, M., Laloui, L., 2008. Effective stress concept in unsaturated soils: Clarification and validation of a unified framework. Int. J. Numer. Anal. Meth. Geomech. 32 (7), 771–801.
Philip, J.R., De Vries, D.A., 1957. Moisture movement in porous materials under temperature gradients. Transactions of the American Geophysical Union 38 (2), 222. https://doi.org/10.1029/TR038i002p00222.
Qiao, Y., Xiao, Y., Laloui, L., Ding, W., He, M., 2019. A double-structure hydromechanical constitutive model for compacted bentonite. Comput. Geotech. 115, 103173. https://doi.org/10.1016/j.compgeo.2019.103173.
Revil, A., Lu, N., 2013. Unified water isotherms for clayey porous materials. Water Resour. Res. 49 (9), 5685–5699.
Romero, E., Vaunat, J., 2000. Retention curves of deformable clays. In Experimental evidence and theoretical approaches in unsaturated soils. CRC Press, pp. 99–114.
Romero, E., Jommi, C., 2008. An insight into the role of hydraulic history on the volume changes of anisotropic clayey soils. Water Resour. Res. 44 (5) https://doi.org/10.1029/2007WR006558.
Rosone, M., Airò Farulla, C., Ferrari, A., 2016. Shear strength of a compacted scaly clay in variable saturation conditions. Acta Geotech. 11 (1), 37–50.
Saiyouri, N., Tessier, D., Hicher, P.Y., 2004. Experimental study of swelling in unsaturated compacted clays. Clay Miner. 39 (4), 469–479.
Sánchez, M., Gens, A., do Nascimento Guimarães, L., Olivella, S., 2005. A double structure generalized plasticity model for expansive materials. Int. J. Numer. Anal. Meth. Geomech. 29 (8), 751–787.
Schrefler, B.A., 1984. The finite element method in soil consolidation (with applications to surface subsidence). Ph.D. Thesis. University College of Swansea.
Sedighi, M., Thomas, H.R., 2014. Micro porosity evolution in compacted swelling clays—A chemical approach. Appl. Clay Sci. 101, 608–618.
Seiphoori, A. 2014. Thermo-hydro-mechanical characterisation and modelling of MX80 granular bentonite. PhD thesis EPFL Lausanne.
Seiphoori, A., Ferrari, A., Laloui, L., 2014. Water retention behaviour and microstructural evolution of MX-80 bentonite during wetting and drying cycles. Géotechnique 64 (9), 721–734.
Sellin, P., Leupin, O.X., 2013. The use of clay as an engineered barrier in radioactive-waste management–a review. Clays Clay Miner. 61 (6), 477–498.
Sposito, G., Prost, R., 1982. Structure of water adsorbed on smectites. Chem. Rev. 82 (6), 553–573.
Tang, A.M., Cui, Y.J., 2010. Experimental study on hydro-mechanical coupling behaviours of highly compacted expansive clay. J. Rock Mech. Geotech. Eng. 2 (1), 39–43.
Van Eekelen, H.A.M., 1980. Isotropic yield surfaces in three dimensions for use in soil mechanics. Int. J. Numer. Anal. Meth. Geomech. 4 (1), 89–101.
van Genuchten, M.T., 1980. A closed-form equation for predicting the hydraulic conductivity of unsaturated soils 1. Soil Sci. Soc. Am. J. 44 (5), 892–898.
Vilarrasa, V., Parisio, F., Laloui, L., 2017. Strength evolution of geomaterials in the octahedral plane under nonisothermal and unsaturated conditions. Int. J. Geomech. 17 (7), 04016152. https://doi.org/10.1061/(ASCE)GM.1943-5622.0000851.
Villar, M.V., 2005. MX-80 Bentonite. Thermal-Hydro-Mechanical Characterisation Performed at CIEMAT in the Context of the Prototype Project (No. CIEMAT–1053). Centro de Investigaciones Energeticas.
Villar, M.V., 2007. Water retention of two natural compacted bentonites. Clays Clay Miner. 55 (3), 311–322.
Villar, M.V., Gómez-Espina, R., Gutiérrez-Nebot, L., 2012. Basal spacing of smectite in compacted bentonite. Appl. Clay Sci. 65, 95–105.
Wheeler, S.J., Sharma, R.S., Buisson, M.S.R., 2003. Coupling of hydraulic hysteresis and stress–strain behaviour in unsaturated soils. Géotechnique 53 (1), 41–54.
Yong, R.N., 1999. Soil suction and soil-water potentials in swelling clays in engineered clay barriers. Eng. Geol. 54 (1-2), 3–13.
Zhang, C., Lu, N., 2018. What is the range of soil water density? Critical reviews with a unified model. Rev. Geophys. 56 (3), 532–562.
Zhou, A.-N., Sheng, D., Sloan, S.W., Gens, A., 2012a. Interpretation of unsaturated soil behaviour in the stress–saturation space, I: volume change and water retention behaviour. Comput. Geotech. 43, 178–187.
Zhou, A.-N., Sheng, D., Sloan, S.W., Gens, A., 2012b. Interpretation of unsaturated soil behaviour in the stress–saturation space: II: constitutive relationships and validations. Comput. Geotech. 43, 111–123.
Zhou, A., Wu, S., Li, J., Sheng, D., 2018. Including degree of capillary saturation into constitutive modelling of unsaturated soils. Comput. Geotech. 95, 82–98.